analytical chemistry

Article

Cite This: Anal. Chem. 2018, 90, 9838−9844

pubs.acs.org/ac

Point-and-Shoot Strategy for Identification of Alcoholic Beverages

Zelun Li,[†] Xuling Chang,[‡] Ying Wang,[†] Changting Wei,[†] Juan Wang,[†] Kelong Ai,*[,†] Ye Zhang,*[,‡] and Lehui Lu*[,†]

[†]State Key Laboratory of Electroanalytical Chemistry, Changchun Institute of Applied Chemistry, Chinese Academy of Sciences, 5625 Renmin Street, Changchun 130022, China

[‡]State Key Laboratory of Applied Optics, Changchun Institute of Optics, Fine Mechanics and Physics, Chinese Academy of Sciences, Changchun East Nanhu Road No. 3888, Changchun 130033, China

Supporting Information

ABSTRACT: The lack of point-and-shoot detection methods of alcoholic beverages (ABs) available for ordinary people is a common cause of the overflow of various counterfeit ABs. Here, we, for the first time, provide a point-and-shoot identification for ABs via a smartphone. Using density functional theory, we find the binding ability of an ethylenediamine-functionalized polydiacetylene (P4) can reach a desirable trade-off among organic molecules in ABs. We therefore construct a versatile array consisting of P4 with different concentrations, which is able to generate unique color response patterns toward different ABs. The color response patterns are further analyzed by a custom-designed image processing algorithm based on machine learning. Finally, the identification of ABs can be achieved by capturing and analyzing the color pattern using an imaging recognition programmer on a smartphone, and the entire process is as fast as quick response (QR) code scanning. Our point-and-shoot strategy makes the identification of ABs accessible to every mobile phone user.

The safety issue of alcoholic beverages (ABs) has fueled an ever-growing demand to develop cost-effective methods that can provide rapid and on-site identification of counterfeit ABs. It is estimated that the turnover of counterfeit ABs worldwide has exceeded $2500 billion in 2014, according to a report by the World Health Organization (WHO).[1] Importantly, counterfeit ABs can lead to long-term adverse effects on human health, such as liver and kidney problems, permanent blindness, and even death. Conventional approaches to ABs identification mainly involve gas chromatography−mass spectrometry (GC/MS) analysis, which enables qualitative analysis of the composition of ABs.[2] These methods, nevertheless, often require bulky equipment, skilled technicians, and extensive sample pretreatment, making them difficult to use for rapid and on-site identification of ABs.

The challenge toward achieving the above aim mainly derives from the fact that different ABs, even the sub-brands of the same AB, are characterized by their unique chemical constituents and/or different ingredient's proportion. Much effort has been made to develop novel probes for identification of ABs through detection of some specific molecules (e.g., tannic acids, aldehydes, or others) in ABs.[3,4] These methods are quite successful in detecting one specific kind of AB but are unsuitable to identify different kinds of ABs. To address this issue, a pioneering colorimetric sensor array consisting aniline and phenylhydrazine dyes has been devised.[5] Tens of array elements are required in this assay to enable the efficient detection and identification of different ABs, which leads to complicated visual readout. Therefore, the development of a rapid and convenient means to convert the complex analysis results into qualitative readout represents another challenge for on-site and rapid identification of counterfeit ABs.

We reasoned that studies of the mechanism underlying the mammalian olfactory system could offer a route to overcome these challenges. Previous reports revealed that such mechanism involved the generation of a "composite response pattern" by cross-reactive bioelectrical sensors under stimulation of odorants, followed by decoding with the brain to produce the information about the specific composition of objects through a procedure called transduction.[6] With this in mind, we focus our attention on the supramolecular conjugated polymers polydiacetylenes (PDA),[7−19] a class of more sensitive colorimetric material than conventional dyes in response to stimuli. Using density functional theory (DFT), we here found that carefully designing and screening a PDA-based probe might allow for the production of unique "color response patterns" toward different ABs. Proof-of-concept investigations demonstrated that a versatile array composed of an ethylenediamine-functionalized PDA with different concentrations could generate characteristic color response patterns toward different ABs. These patterns could be extracted and analyzed by a custom-designed image processing algorithm

Received: April 27, 2018
Accepted: July 31, 2018
Published: July 31, 2018

DOI: 10.1021/acs.analchem.8b01895
Anal. Chem. 2018, 90, 9838−9844

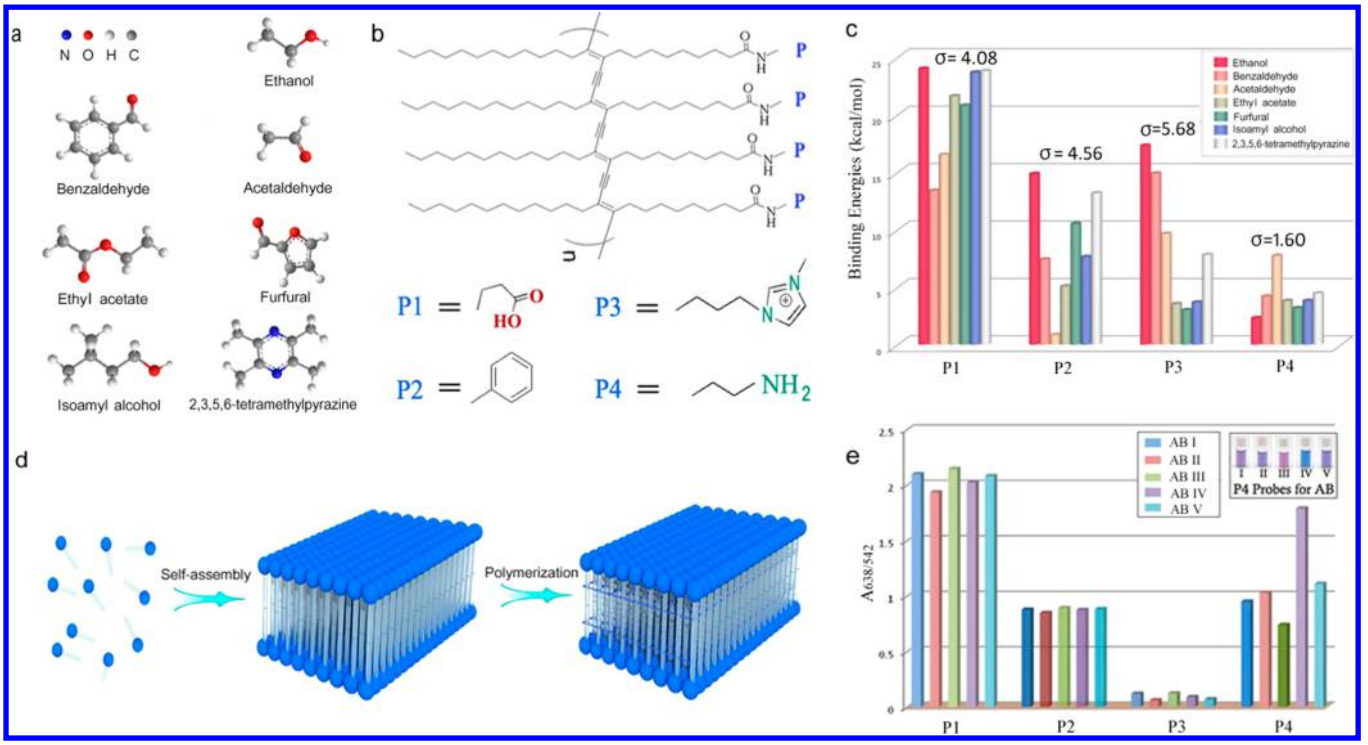

Figure 1. Selection of the probe. (a) Chemical structures of the small organic molecules in ABs. (b) Schematic diagram of aminobutyric acid (P1)-, aniline (P2)-, imidazolium (P3)-, and ethylenediamine (P4)-functionalized PDAs. (c) The binding energies of P1−P4 with small organic molecules in ABs ($|\Delta G_{Prob*}|$). (d) Schematic illustration of self-assembly and polymerization of the monomer. (e) The changes in the ratio of $A_{638/542}$ of each probe in response to five different ABs. Inset is the color responses of P4 to five ABs.

based on machine learning, enabling accurate reporting the required details of ABs on the smartphone within 1 min.

RESULTS AND DISCUSSION

Design Optimization of the PDA Derivate Based Probe. Determination of the ABs compositions is necessary for designing the PDA-based probe. Hence, we first performed GC/MS analysis to test the detailed compositions of ABs with 16 commercially available ABs as examples. GC/MS showed that ABs mainly contained a large amount of ethanol, and six other kinds of small organic molecules at parts-per-million (ppm) levels (Figure 1a) (Table S1). Considering the structural characters of these small organic molecules and the physicochemical properties of the probes, aminobutyric acid (P1)-, aniline (P2)-, imidazolium (P3)-, and ethylenediamine (P4)-functionalized PDAs were chosen carefully as candidate probes (Figure 1b).[20−24]

The binding ability of the probe with molecule is highly correlated with the binding/formation energy, ΔG_{Prob*}. Thus, we carried out DFT simulations to get the probe binding sites and their corresponding ΔG_{Prob*} (Figures S1−S7).[25−27] Given the GC/MS results that showed the volume of ethanol was greater than that of other organic molecules, we believed an intricate trade-off between the binding ability of probe with ethanol and that with other organic molecules was the key for a probe to provide a comprehensive response. Namely, a lower value of $|\Delta G_{Prob*}|$ with ethanol than that with other organic molecules was required because a high binding ability of probe with ethanol might sequester accessible binding sites for other organic molecules. Moreover, a smaller standard deviation of $|\Delta G_{Prob*}|$ should be acquired to balance the binding opportunities for organic molecules. Theoretical results suggested that P4 was a desirable candidate probe for the identification of ABs (Figure 1c).

Encouraged by the result of DFT simulations, proof-of-concept investigations were carried out by using five commercially available ABs as samples. Briefly, the P4 monomers were synthesized and dissolved in TAPS buffer (20 mM, pH 7.7), and subsequently polymerized to its stable polymer under UV irradiation (Figure 1d). Upon exposure to these samples, diverse color changes of P4 were observed by the naked eye within 1 min, with an obvious blue shift of the absorption maximum from 638 to 542 nm in the UV−vis spectrum (Figures S8−S12). To quantify the colorimetric response, the absorption ratio ($A_{638/542}$) was monitored. In control experiments, P1−P3 were also prepared and demonstrated negligible difference in response to the samples, well-consistent with the theoretical calculation (Figure 1e). In the preliminary experiment, concentration optimization of the probe has been conducted. Negligible color change (from blue to purple) was observed upon exposure of the probes with high concentration (>1.73 mM) to the tested ABs, while almost the same color change could be noticed (from blue to red) upon exposure of the probe with low concentration (<0.51 mM) to various ABs (Figure S13). Thus, a trade-off between low concentration and high concentration is needed to distinguish the ABs effectively. A versatile array (Figure S14) was further fabricated simply by using equal volume (2 mL) of P4 with different concentrations (0.51, 0.86, and 1.73 mM), which were expressed as C1−C3, respectively. In order to quantify differences, the ratios of $A_{638/542}$ of C1−C3 in response to ABs were defined as the values of X, Y, and Z in the three-dimensional (3D) coordinate system, respectively. Accordingly, a characteristic color response pattern and a correspond-

DOI: 10.1021/acs.analchem.8b01895
Anal. Chem. 2018, 90, 9838−9844

ing location in the 3D coordinate system would be generated with this assay (Figure 2).

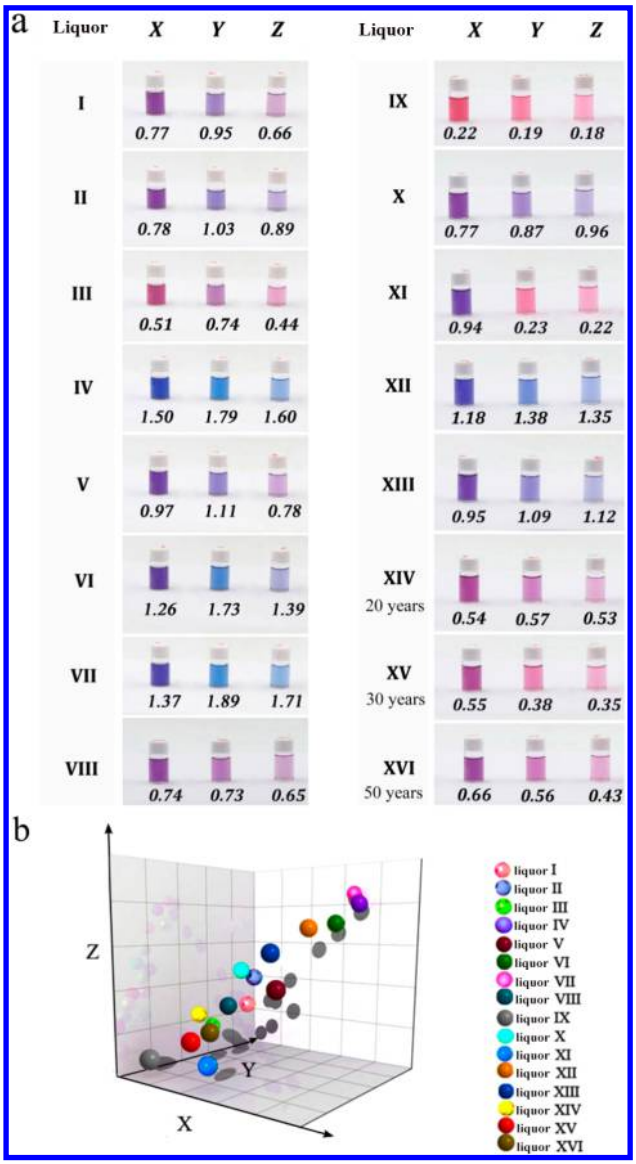

Figure 2. Discrimination of 16 kinds of liquors. (a) Characteristic color response patterns. (b) 3D coordinates.

Performance Investigation of the Single-Sensing Element Array. To demonstrate the suitability of this array, we tested 29 kinds of ABs including Chinese liquor (According to their aroma, taste, and manufacturing process, Chinese liquors were mainly divided into seven kinds of classification) (Table1), vodka, rum, white wine, sake, and counterfeits (Figures S15–S17). Impressively, naked-eye differentiation of these ABs could be achieved using our probe array, with specific 3D coordinates. The result established that our single-sensing element platform can not only discriminate among ABs of different regions and/or kinds but is also well-suited for differentiating among the same kind of ABs. Table 1 summarizes the liquors selected for investigation. It is also worth noting that even the liquors with the same raw materials (e.g., III, VII, VIII), and/or with the same content of ethanol (e.g., I, II, VII), and/or with the same classification (e.g., VII, VIII, IX) could be easily distinguished by using the probe array. Specially, discriminating liquors with the same brand but different ages (20 years, XIV; 30 years, XV; and 50 years, XVI) is a challenging task because of their highly similar chemical constitutes as confirmed by GC/MS analysis. Gratifyingly, the addition of equal volume of AB (2 mL) to each array element yielded the characteristic color response patterns (Figure 2a), which were also well-evidenced by their corresponding *X*, *Y*, *Z* values (Figure 2b).

Table 1. Detailed Information of Sixteen Kinds of Liquors

liquor	pH	EtOH [%]	classification	raw materials
I	3.96	42	light	sorghum
II	3.80	42	light	sorghum corn
III	4.49	48	strong	sorghum barley wheat
IV	3.60	45	light	sorghum barley pea
V	3.79	52	strong	sorghum
VI	5.06	56	light	sorghum wheat
VII	3.87	42	strong	sorghum barley wheat
VIII	4.14	45	strong	sorghum barley wheat
IX	3.99	52	strong	sorghum wheat
X	4.26	50	phoenix	sorghum wheat pea
XI	4.09	53	strong	sorghum rice wheat
XII	3.86	52	light	sorghum wheat
XIII	4.20	52	light	sorghum wheat
XIV	4.30	52	strong	sorghum
XV	4.22	52	strong	sorghum
XVI	4.26	52	strong	sorghum

Given the excellent performance of the probe array for ABs identification, we next proceeded to test its repeatability and stability, crucial factors in determining whether this probe array could be exploited in practical applications. After storage at room temperature for 2 months, it was found that the color of P4 and its UV–vis spectra had no noticeable change. Upon exposure of the probe array to AB (liquor III), the characteristic color response pattern remained stable for at least 1 month. Also, we tested five bottles of the same liquors (ABVIII) purchased from different markets. After mixing the liquors with the probe array, the relative standard deviations for C1, C2, and C3 were 1.16%, 0.98%, and 0.74%, respectively (Figures S18–S20).

Given the excellent sensitivity, repeatability, and stability of the probe array for ABs identification, we ultimately investigated whether the probe array can identify counterfeits ABs, because our ultimate aim is to prevent the overflow of the counterfeit ABs. Five different counterfeit liquor IIIs (F1–F5) provided by the manufacturers were chosen as examples. Upon exposure to the probe array, the characteristic color response patterns of F1–F5 were obviously different from that of the authentic liquor III, which was also well-evidenced by their corresponding *X*, *Y*, *Z* values. These encouraging results suggested that our probe array offered great promise for pinning down counterfeit ABs (Figure S21).

Sensing Mechanism. The mechanism underlying unique color response pattern was first investigated by comparing the color response data of individual components of AB (liquor V), relying on the use of GC/MS analysis. Simultaneously, an artificial liquor was prepared by using the known components. (Notably, there are some unknown substances that could not be detected by GC/MS.) As expected, none of the color responses of individual components was identical with that of liquor V, whereas the color response of the artificial liquor was highly close to that of liquor V, hence confirming that the color

DOI: 10.1021/acs.analchem.8b01895
Anal. Chem. 2018, 90, 9838–9844

change of P4 was due to the combinatorial effect triggered by different organic molecules in ABs, which was in good agreement with DFT calculations (Table S2) (Figure S22).

It is generally accepted that the side chain of PDA could impose a mechanical strain on its backbone during the polymerization process of PDA monomers, because of the geometric constraints produced by hydrogen-bond or van der Waals interactions between the side chains. The disruption of interactions between the side chains enables the release of mechanical force on its backbone, and hence causes the transformation in the electronic structure of its backbone.[28−35] To determine the mechanism of color change of P4, transmission electron microscopy (TEM) was used. As shown in Figure 3a, P4 had a fibrous structure. Upon exposure

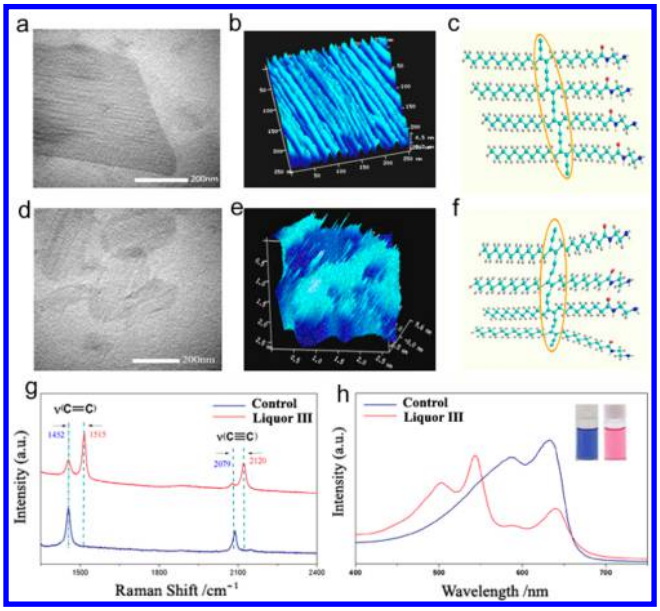

Figure 3. P4 Characterization. (a) TEM image of P4. (b) 3D AFM image of P4. (c) Molecular arrangement model of P4; the conjugate backbone of P4 is circled by the orange oval. (d) TEM image of P4 after addition of liquor III. (e) 3D AFM image of P4 after addition of liquor III. (f) Molecular arrangement model of P4 after addition of liquor III; the conjugate backbone of P4 is circled by the orange oval. (g) Raman spectroscopy of P4 in the presence of 2 mL of liquor III and 2 mL of deionized water. (h) UV−vis spectra of P4 in the presence of 2 mL of liquor III and 2 mL of deionized water. Inset is the photograph of P4 and after adding liquor III.

to AB, the regular arrangement of P4 was obviously destroyed (Figure 3d). Atomic force microscope (AFM) data further confirmed such morphological change during the chromatic transition of P4 triggered by small organic molecules in ABs (Figure 3, parts b and e) (Figure S23).[36−39] The transformation in the electronic structure of its backbone could be evidenced by Raman spectrum data. Both the ν(C═C) peak and the ν(C≡C) peak shifted to higher frequencies (Figure 3, parts c and f). Likewise, this result was consistent with the blue shift of absorption maximum in the UV−vis spectrum, which was an indication of a decrease in the π-electron delocalization of P4 (Figure 3, parts g and h).[40−42] Hence, we concluded that the addition of ABs could promote the conformation change in the backbone of P4, which ultimately led to its color change.

Construction of a Color Pattern Reader APP on the Smartphone. The development of a portable device to analyze ABs and provide immediate identification results at any geographical place is of great significance for preventing the overflow of counterfeit ABs in the global market. Artificial intelligence can not only avoid subjective analysis but also identify minor differences that fail to be observed by the naked eye. We therefore analyzed the color response patterns obtained from the highly sensitive sensor array of P4 using a mobile imaging platform on a smartphone. We have used an industrialized camera obscura containing a light-emitting diode (LED) to collect all the standard images. In addition to the camera, an object detection algorithm based on machine learning was designed and implemented on a smartphone under the Android system.

Briefly, the ABs detection can be divided into two steps. First, a region-based convolutional neural network (Faster-RCNN) needs to be used for AB detecting and extracting bounding boxes for every single color response pattern (Figure 4a). Next, we used k-nearest neighbor (KNN) to classify the

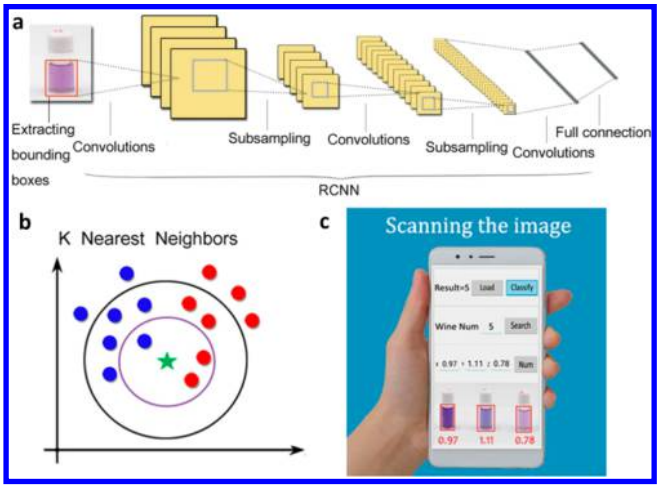

Figure 4. Color pattern reader APP. (a) Schematic diagram of the Faster-RCNN. (b) Schematic diagram of k-nearest neighbors. (c) Photographs of the reader of the color pattern on the smartphone.

color pattern into its real type with the precalculated value of X, Y, and Z data which is saved as the standard data of the ABs tested, guaranteeing the accurate identification of ABs. The KNN algorithm can find the most nearest k neighbors and classify the input value using the function below:

$$f(x_q) = \text{argmax}_{v \in V} \sum_{i=1}^{k} \delta(v, f(x_i))$$

Here, if $\delta(|a-b|) < \varepsilon$, then $\delta(|a-b|) = 1$; otherwise, $\delta(|a-b|) = 0$. x_q is the input value. Function $f(x)$ calculated the class number of x. The key to the KNN procedure is the voting. By calculating the distance of data items, the data set we prepared voted the correct answer (Figure 4b).[43]

In the detection part, a state-of-the-art object detection algorithm called Faster-RCNN was used, which is built upon the theory of deep learning. The Faster-RCNN model was obtained by inputting a bunch of color response patterns that are labeled one by one into the Faster-RCNN training system implemented based on Caffe. Faster-RCNN contains a region proposal network (RPN) and a detection network. The RPN is a fully convolutional network (FCN), which can generate a batch of region proposals with objectness score and bounding boxes. In the RPN stage, the Zeiler and Fergus model (ZF) or

DOI: 10.1021/acs.analchem.8b01895
Anal. Chem. 2018, 90, 9838−9844

the Simonyan and Zisserman model (VGG) can be used. ZF model has five convolutional (conv) layers, while VGG model has 13 conv layers. The ZF model was selected for our detection, as it is not complicated and only has one object class and background. Another reason for choosing the ZF model is the convolution layers between the RPN and the detection network. A simpler model structure will be easier to converge. For training RPN, a loss function was minimized, according to the equation below:

$$L(\{p_i\}, \{t_i\}) = \frac{1}{N_{cls}} \sum_i L_{cls}(p_i, p_i^*) + \lambda \frac{1}{N_{reg}} \sum_i p_i^* L_{reg}(t_i, t_i^*)$$

where i is the index of an object location in a training batch and p_i is the predicted result of location i being an object. Value p_i^* represents the object ground truth. t_i is the predicted bounding box, and t_i^* is the ground-truth bounding box. The classification loss, L_{cls}, is log loss, and the regression loss, L_{reg}, is the robust loss function (smooth L_1) defined in. The output architecture is implemented with an $n \times n$ conv layer followed by two 1×1 conv layers, which output the objectness score and bounding box, respectively. The output values of the two conv layers are refined by ReLU layers.[44,45]

Once we have trained the RPN, we can use the proposals generated to train the detection network. Then, we shared the conv layers between the RPN and the detection network as described in the alternating optimization training process. In this step, the conv layers trained from the detection network to the RPN were shared, because the detection conv layers have a stronger feature for the region proposal task. Both the RPN and detection network can be trained end to end by back-propagation and stochastic gradient descent (SGD).The training was run on a GPU server with two NVIDIA TITAN-X GPUs, one i7-6800k CPU, and 64 GB memory. The model was trained 20 000 iteration, and a final model was obtained with an object detecting accuracy of nearly 100%.

Consider that, in practical applications, the recognition would be affected by the variations in the condition of taking the images, such as the quality of the ambient light, etc. To address this problem, a pretreatment procedure of image called color calibration (ColorCalib) was designed. A ministudio was used to collect the photographs shown in the above experiment, which is an ideal illumination condition to get the standard the photographs (Figure S24). Thus, the photographs demonstrated in this study can serve as the standard photographs. In practical applications, we recapture the control group of the probe array (only adding water) under the real condition first, which was used to compare with the standard photograph of the control group to get the differentiation of illumination of them. Formally, if we use RGB to describe the color of images, the differentiation can be represented as

$$\nabla_{COLOR} = (\nabla_R, \nabla_G, \nabla_B)$$

To get a relatively stable value, we select the central 10×10 pixels of each of the array elements. Therefore, ∇_{COLOR} will be $9 \times 10 \times 10$ (3 channels, 3 array elements) matrix. Next, we capture the photograph for detection (adding the AB tested) under the same illumination. The color in the detection photograph will be calibrated to the standard color through subtracting ∇_{COLOR} (Figure S25). In this way, the variations in the condition of taking the images would be eliminated.

Upon exposure of the AB to the highly sensitive sensor array of P4, each AB would show a unique color response pattern due to its characteristic composition, just as a human fingerprint. The ABs identification could be achieved by the following simple steps: (i) mixing the probe array with the samples, (ii) taking photos of the color pattern image, and (iii) scanning the color pattern image on the smartphone, similar to QR code scanning. The AB will then be identified by the APP, giving an accurate qualitative result through analyzing the color patterns of different ABs. The entire process is similar to the quick response (QR) code scanning. We have shown that our smartphone-assisted semiautomatic approach can identify 29 kinds of samples, including vodka, rum, white wine, sake, and counterfeits, and provide the user a result with ~100% accuracy. For real-world applications, the details on ABs, such as brand, year, type, batch, and authenticity could be acquired immediately using this platform (Figure 4c).[46−52]

EXPERIMENTAL SECTION

Materials and Instrumentation. 10,12-Pentacosadiynoic acid (PCDA) was obtained from Alfa Aesar. Other reagents were purchased from Sigma-Aldrich. All organic solvents were obtained from BEIJING chemical works which were used without further purification. TEM images of polymer P4 were obtained by using a JEOL 2000-FX transmission electron microscopy. ^{1}H and ^{13}C spectra were collected on a Bruker AV400 spectrometer. Electrospray ionization mass spectrometry (ESI-MS) spectra were obtained by a Bruker MALDI-TOF/TOF autoflex III. Raman spectra were excited using a 632 nm diode laser controller and obtained by a LabRAM ARAMIS Raman spectroscope system (Scientific HORIBA) equipped with a charge-coupled device (CCD) detector. AFM images were collected on a multimode 8 AFM system (Veeco, U.S.A.). Photographic images were collected by using a PENTAX *ISTD digital camera. UV−vis spectra were obtained by using a Varian Cary 50 UV−vis spectrophotometer.

Synthesis of the P4 Monomer. The monomers were synthesized according to previous literatures.[20,23,24] ^{1}H NMR (400 MHz, $CDCl_3$): δH 0.88 (t, J = 6.8 Hz 3H), 1.42 (m, 32H), 2.18 (t, J = 7.6 Hz 2H), 2.24 (t, J = 6.8 Hz 4H), 2.83 (t, J = 5.7 Hz 2H), 3.31 (q, J = 5.8 Hz 2H), 5.94 (brs, 1H) ppm. ^{13}C NMR (400 MHz, $CDCl_3$): δC 173.5, 77.6, 77.4, 65.3, 65.2, 41.6, 41.3, 36.8, 31.9, 29.6, 29.6, 29.5, 29.4, 29.3, 29.2, 29.1, 28.9, 28.9, 28.6, 28.4, 28.4, 28.1, 25.7, 22.7, 19.2, 19.2, 14.1 ppm. ESI-MS m/z = 417.4 $[M + H]^+$, 439.3 $[M + Na]^+$, and 455.3 $[M + K]^+$.

DFT Simulation. All calculations performed in this study were using DFT with the program package of DMol3 in the Materials Studio of BIOVIA Inc. The exchange-correlation energy was described through generalized gradient approximation (GGA) by the Perdew−Burke−Ernzerhof (PBE) function. All-electron relativistic and double-numerical basis sets with polarization functional (DNP 4.4) were adopted to all elements.

Preparation of the Probe Array. P4 monomer was added to a aqueous solution (TAPS, 20 mM, pH 7.7) for obtaining monomer concentrations of 0.51, 0.86, and 1.73 mM, respectively (C1, C2, C3). The samples were sonicated at 75−80 °C for 50 min, and then stored at 4 °C for overnight. Polymerization of P4 monomer was conducted by irradiating the samples with 254 nm UV light (6 W) for 18 min. The

DOI: 10.1021/acs.analchem.8b01895
Anal. Chem. 2018, 90, 9838−9844

probe array is consists of equal volume (2 mL) of the P4 probes in three different concentrations after polymerization.

Detection of Alcoholic Beverages. A total of 6 mL of the alcoholic drink (2 mL for each array element) was added to the probe array. The data were collected after 2 min.

Implementation Details. We developed our experiment application using C++ programming language under a cross-platform user interface framework Qt. A few OpenCV modules have been used for some basic image processing work. The training system we used is Faster-RCNN, which was developed by Ross Girshick using Python and C++. We first developed our program on a desktop, then migrated it to the Android system. The cellphone we used in our experiment is running the Android operating system with Kernel version 3.10.74.

CONCLUSION

In summary, we provided a smartphone-based strategy to enable the identification of ABs in any environment. This approach offers several advantages over current ABs identification techniques. First, this approach does not need any sample pretreatment and complicated instruments, which makes rapid identification of ABs accessible to people who own a smartphone. Second, this approach exhibits a performance, reproducibility, and accuracy comparable to that of the GC/MS benchmark. Finally, counterfeit ABs can be identified within 1 min, which makes this approach promising for addressing the safety issue of ABs. This approach may be also applicable to identify a wider range of liquid composition (wastewater, fruit juice beverages, pesticide). Moreover, our novel design is a promising tool for sensing, responding, and reporting complex substances for both laboratory and point-of-care uses.

ASSOCIATED CONTENT

Supporting Information

The Supporting Information is available free of charge on the ACS Publications website at DOI: 10.1021/acs.analchem.8b01895.

Simulation of binding sites, polymerization, UV−vis, NMR, and mass spectra, stability and repeatability tests, color patterns, mechanism of the color response, AFM analysis, GC/MS results, and color response data (PDF)

AUTHOR INFORMATION

Corresponding Authors

*E-mail: klai@ciac.ac.cn.
*E-mail: zhangye@ciomp.ac.cn.
*E-mail: lehuilu@ciac.ac.cn. Phone: +86-43185262697. Fax: +86-43185262406.

ORCID

Lehui Lu: 0000-0003-1343-0213

Notes

The authors declare no competing financial interest.

ACKNOWLEDGMENTS

We gratefully acknowledge the financial support received from the National Key Research and Development Program of China (no. 2016YFA0203200), the National Natural Science Foundation of China (nos. 21635007, 21721003, 21605137), the Youth Innovation Promotion Association of the Chinese Academy of Sciences (nos. 2014201, 2016201), the Natural Science Foundation of Jilin Province (20160101321JC), the K. C. Wong Education Foundation, and the Computing Center of Jilin Province.

REFERENCES

(1) Rehm, J.; Gmel, G.; Hasan, O. S. M.; Imtiaz, S.; Popova, S.; Probst, C.; Roerecke, M.; Room, R.; Samokhvalov, A. V.; Shield, K. D.; Shuper, P. A. *Addiction* **2017**, *112*, 1687−1688.
(2) Wisniewska, P.; Dymerski, T.; Wardencki, W.; Namiesnik, J. *J. Sci. Food Agric.* **2015**, *95*, 2159−2166.
(3) Han, J.; Bender, M.; Seehafer, K.; Bunz, U. H. F. *Angew. Chem., Int. Ed.* **2016**, *55*, 7689−7692.
(4) Heller, M.; Vitali, L.; Oliveira, M. A. L.; Costa, A. C. O.; Micke, G. A. *J. Agric. Food Chem.* **2011**, *59*, 6882−6888.
(5) Li, Z.; Fang, M.; LaGasse, M. K.; Askim, J. R.; Suslick, K. S. *Angew. Chem., Int. Ed.* **2017**, *56*, 9860−9863.
(6) Dunkel, A.; Steinhaus, M.; Kotthoff, M.; Nowak, B.; Krautwurst, D.; Schieberle, P.; Hofmann, T. *Angew. Chem., Int. Ed.* **2014**, *53*, 7124−7143.
(7) Charych, D.; Nagy, J.; Spevak, W.; Bednarski, M. *Science* **1993**, *261*, 585−588.
(8) Lee, J.; Pyo, M.; Lee, S. H.; Kim, J.; Ra, M.; Kim, W. Y.; Park, B. J.; Lee, C. W.; Kim, J. M. *Nat. Commun.* **2014**, *5*, 3736.
(9) Lee, K. M.; Moon, J. H.; Jeon, H.; Chen, X. Q.; Kim, H. J.; Kim, S.; Kim, S. J.; Lee, J. Y.; Yoon, J. *J. Mater. Chem.* **2011**, *21*, 17160−17166.
(10) Charych, D. H.; Nagy, J. O.; Spevak, W.; Bednarski, M. D. *Science* **1993**, *261*, 585−588.
(11) Kim, T. H.; Lee, B. Y.; Jaworski, J.; Yokoyama, K.; Chung, W. J.; Wang, E.; Hong, S.; Majumdar, A.; Lee, S. W. *ACS Nano* **2011**, *5*, 2824−2830.
(12) Lu, Y. F.; Yang, Y.; Sellinger, A.; Lu, M. C.; Huang, J. M.; Fan, H. Y.; Haddad, R.; Lopez, G.; Burns, A. R.; Sasaki, D. Y.; Shelnutt, J.; Brinker, C. J. *Nature* **2001**, *411*, 617−617.
(13) Lee, S.; Lee, J.; Lee, M.; Cho, Y. K.; Baek, J.; Kim, J.; Park, S.; Kim, M. H.; Chang, R.; Yoon, J. *Adv. Funct. Mater.* **2014**, *24*, 3699−3705.
(14) Sun, A. W.; Lauher, J. W.; Goroff, N. S. *Science* **2006**, *312*, 1030−1034.
(15) Wang, Y.; Pei, H. W.; Jia, Y.; Liu, J. H.; Li, Z. L.; Ai, K. L.; Lu, Z. Y.; Lu, L. H. *J. Am. Chem. Soc.* **2017**, *139*, 11616−11621.
(16) Berman, A.; Ahn, D. J.; Lio, A.; Salmeron, M.; Reichert, A.; Charych, D. *Science* **1995**, *269*, 515−518.
(17) Wu, D.; Chen, L.; Kwon, N.; Yoon, J. *Chem.* **2016**, *1*, 674−698.
(18) Batchelder, D. N.; Evans, S. D.; Freeman, T. L.; Haussling, L.; Ringsdorf, H.; Wolf, H. *J. Am. Chem. Soc.* **1994**, *116*, 1050−1053.
(19) Jordan, R. S.; Li, Y. L.; Lin, C. W.; McCurdy, R. D.; Lin, J. B.; Brosmer, J. L.; Marsh, K. L.; Khan, S. I.; Houk, K. N.; Kaner, R. B.; Rubin, Y. *J. Am. Chem. Soc.* **2017**, *139*, 15878−15890.
(20) Eaidkong, T.; Mungkarndee, R.; Phollookin, C.; Tumcharern, G.; Sukwattanasinitt, M.; Wacharasindhu, S. *J. Mater. Chem.* **2012**, *22*, 5970−5977.
(21) Yoon, B.; Lee, S.; Kim, J. M. *Chem. Soc. Rev.* **2009**, *38*, 1958−1968.
(22) Jonas, U.; Shah, K.; Norvez, S.; Charych, D. H. *J. Am. Chem. Soc.* **1999**, *121*, 4580−4588.
(23) Yoon, J.; Jung, Y. S.; Kim, J. M. *Adv. Funct. Mater.* **2009**, *19*, 209−214.
(24) Chen, X.; Kang, S.; Kim, M. J.; Kim, J.; Kim, Y. S.; Kim, H.; Chi, B.; Kim, S. J.; Lee, J. Y.; Yoon, J. *Angew. Chem., Int. Ed.* **2010**, *49*, 1422−1425.
(25) Delley, B. *J. Chem. Phys.* **2000**, *113*, 7756−7764.
(26) Perdew, J. P.; Burke, K.; Ernzerhof, M. *Phys. Rev. Lett.* **1996**, *77*, 3865−3868.
(27) Delley, B. *J. Chem. Phys.* **1990**, *92*, 508−517.
(28) Mosley, D. W.; Sellmyer, M. A.; Daida, E. J.; Jacobson, J. M. *J. Am. Chem. Soc.* **2003**, *125*, 10532−10533.

DOI: 10.1021/acs.analchem.8b01895
Anal. Chem. 2018, 90, 9838−9844

(29) Olsen, A. W.; Kafafi, Z. H. *J. Am. Chem. Soc.* **1991**, *113*, 7758−7760.
(30) Paley, M. S.; Frazier, D. O.; Abdeldeyem, H.; Armstrong, S.; Mcmanus, S. P. *J. Am. Chem. Soc.* **1995**, *117*, 4775−4780.
(31) Yoon, B.; Ham, D.-Y.; Yarimaga, O.; An, H.; Lee, C. W.; Kim, J.-M. *Adv. Mater.* **2011**, *23*, 5492−5497.
(32) Reichert, A.; Nagy, J. O.; Spevak, W.; Charych, D. *J. Am. Chem. Soc.* **1995**, *117*, 829−830.
(33) Scott, L. T.; Cooney, M. J.; Johnels, D. *J. Am. Chem. Soc.* **1990**, *112*, 4054−4055.
(34) Song, J.; Cisar, J. S.; Bertozzi, C. R. *J. Am. Chem. Soc.* **2004**, *126*, 8459−8465.
(35) Maeda, K.; Hong, L.; Nishihara, T.; Nakanishi, Y.; Miyauchi, Y.; Kitaura, R.; Ousaka, N.; Yashima, E.; Ito, H.; Itami, K. *J. Am. Chem. Soc.* **2016**, *138*, 11001−11008.
(36) Wu, P. J.; Kuo, S. Y.; Huang, Y. C.; Chen, C. P.; Chan, Y. H. *Anal. Chem.* **2014**, *86*, 4831−4839.
(37) Kuo, S. Y.; Li, H. H.; Wu, P. J.; Chen, C. P.; Huang, Y. C.; Chan, Y. H. *Anal. Chem.* **2015**, *87*, 4765−4771.
(38) Diegelmann, S. R.; Hartman, N.; Markovic, N.; Tovar, J. D. *J. Am. Chem. Soc.* **2012**, *134*, 2028−2031.
(39) Xu, Y. W.; Smith, M. D.; Geer, M. F.; Pellechia, P. J.; Brown, J. C.; Wibowo, A. C.; Shimizu, L. S. *J. Am. Chem. Soc.* **2010**, *132*, 5334−5335.
(40) Zhu, L. L.; Tran, H.; Beyer, F. L.; Walck, S. D.; Li, X.; Agren, H.; Killops, K. L.; Campos, L. M. *J. Am. Chem. Soc.* **2014**, *136*, 13381−13387.
(41) Ahn, D. J.; Kim, J. M. *Acc. Chem. Res.* **2008**, *41*, 805−816.
(42) Phollookin, C.; Wacharasindhu, S.; Ajavakom, A.; Tumcharern, G.; Ampornpun, S.; Eaidkong, T.; Sukwattanasinitt, M. *Macromolecules* **2010**, *43*, 7540−7548.
(43) Zeiler, M. D.; Fergus, R. Visualizing and Understanding Convolutional Networks. In *Computer Vision - ECCV 2014*; Fleet, D., Pajdla, T., Schiele, B., Tuytelaars, T., Eds.; Springer: Cham, Switzerland, 2013; Vol. *8689*, pp 818−833.
(44) Ren, S. Q.; He, K. M.; Girshick, R.; Sun, J. *IEEE Trans. Pattern Anal. Mach. Intell.* **2017**, *39*, 1137−1149.
(45) Wang, D.; Yang, J.; Deng, J. K.; Liu, Q. S. *Signal Process-Image* **2016**, *47*, 476−481.
(46) Zhang, L.; Qi, H. T.; Wang, Y. X.; Yang, L. F.; Yu, P.; Mao, L. Q. *Anal. Chem.* **2014**, *86*, 7280−7285.
(47) Yildirim, A.; Ozturk, F. E.; Bayindir, M. *Anal. Chem.* **2013**, *85*, 6384−6391.
(48) Papai, R.; Sato, R. H.; Nunes, L. C.; Krug, F. J.; Gaubeur, I. *Anal. Chem.* **2017**, *89*, 2807−2815.
(49) Jeong, J. P.; Cho, E.; Yun, D.; Kim, T.; Lee, I. S.; Jung, S. *Polymers* **2017**, *9*, 127.
(50) Gilbert, A.; Yamada, K.; Yoshida, N. *Anal. Chem.* **2013**, *85*, 6566−6570.
(51) Fogwill, M. O.; Thurbide, K. B. *Anal. Chem.* **2010**, *82*, 10060−10067.
(52) Chandrasekhar, A.; Kim, C. S.; Naji, M.; Natarajan, K.; Hahn, J. O.; Mukkamala, R. *Sci. Transl. Med.* **2018**, *10*, eaap8674.

DOI: 10.1021/acs.analchem.8b01895
Anal. Chem. 2018, 90, 9838−9844